Geosci. Model Dev. Discuss., 7, 1791–1827, 2014
www.geosci-model-dev-discuss.net/7/1791/2014/
doi:10.5194/gmdd-7-1791-2014

Geoscientific Model Development
Discussions
Open Access

Formulation, calibration and validation of the DAIS model (version 1), a simple Antarctic Ice Sheet model sensitive to variations of sea level and ocean subsurface temperature

G. Shaffer[1,2,3,*]

[1]Center for Advanced Research in Arid Zones, La Serena, Chile
[2]Center for Climate and Resilience Research, Santiago, Chile
[3]Niels Bohr Institute, University of Copenhagen, Copenhagen, Denmark
[*]formerly at: Department of Geophysics, University of Concepcion, Concepcion, Chile

Received: 23 February 2014 – Accepted: 3 March 2014 – Published: 18 March 2014

Correspondence to: G. Shaffer (gary.shaffer@ceaza.cl)

Published by Copernicus Publications on behalf of the European Geosciences Union.

Abstract

The Dcess Antarctic Ice Sheet (DAIS) model is presented. Model hindcasts of Antarctic Ice Sheet (AIS) sea level equivalent are forced by reconstructed Antarctic temperatures, global mean sea level and high-latitude, subsurface ocean temperatures, the latter calculated using the Danish Center for Earth System Science (DCESS) Earth System Model forced by reconstructed global mean atmospheric temperatures. The model is calibrated by comparing such hindcasts for different model configurations with paleoreconstructions of AIS sea level equivalent from the last interglacial, the last glacial maximum and the mid-Holocene. The calibrated model is then validated against present estimates of the rate of AIS ice loss. It is found that a high-order dependency of ice flow at the grounding line on water depth there is needed to capture the observed response of the AIS at ice age terminations. Furthermore it is found that a dependency of this ice flow on ocean subsurface temperature by way of ice shelf demise and a resulting buttressing decrease is needed to explain the contribution of the AIS to global mean sea level rise at the last interglacial. When forced and calibrated in this way, model hindcasts of the rate of present day AIS ice loss agree with recent, data-based estimates of this ice loss rate.

1 Introduction

The Antarctic Ice Sheet (AIS) is a major player in the Earth's climate system and is by far the largest depository of fresh water on the planet. Ice stored in the AIS contains enough water to raise sea level by about 58 m and ice loss from Antarctica contributed significantly to sea level high stands during past interglacial periods (Vaughan et al., 2013; Kopp et al., 2009; Naish et al., 2009). There is considerable uncertainty as to the amount the AIS will contribute to future sea level change in response to ongoing global warming (Church et al., 2013).

A broad hierarchy of AIS models have been developed and applied to try to understand the workings of the AIS and to form a robust basis for future projections of the AIS contribution to sea level change (e.g. Huybrechts, 1990; Huybrechts and Wolde, 1999; Oerlemans, 2003; Pollard and De Conto, 2009; Whitehouse et al., 2012). In some cases, AIS models have been coupled to global climate models (e.g. Pollard and DeConto, 2005; Vizcaino et al., 2010). A common feature of the earlier of these models is an increase in AIS ice mass in response to warming as a consequence of increased snow fall. However observations show that the AIS is loosing mass at present (Vaughan et al., 2013).

Two recent advances in our understanding of ice flow at the grounding line have been paving the way for AIS model improvements. First, a detailed study comparing results from boundary layer theory with high resolution numerical modeling showed that ice flux at the grounding line increases sharply with ice thickness there (Schoof, 2007). Second, observations show that ice stream flow increases substantially when an adjoining ice shelf disintegrates, removing associated buttressing of the ice stream (Rignot et al., 2004). Ice shelf disintegration appears to be mainly associated with increased basal melting from increasing subsurface temperatures of the adjoining ocean (Shepherd et al., 2004). This chain of processes has been proposed as a trigger for Heinrich events, explaining why they occur during cold phases of millennial-scale climate variations when the North Atlantic warms at intermediate depths due to shutdowns of the Atlantic Meridional Overturning Circulation (Shaffer et al., 2004). There is considerable support for this interpretation in the ocean sediment record (Marcott et al., 2011).

Here I take a simple modelling approach with recent work by Johannes Oerlemans as my point of departure (Oerlemans, 2003, 2004, 2005). First I consider the mass balance formulations in these publications whereby I correct some errors and make several parameter value adjustments that follow from the consequences of the corrections. Then I consider formulations within this modeling context of the two recent advances discussed above. The new DAIS model is then forced by reconstructed time

GMDD
7, 1791–1827, 2014

series of Antarctic temperature, sea level and subsurface ocean temperature over the last two glacial cycles. Values for the parameters used in the model formulations of the effect on ice flux of grounding line ice thickness and basal melting are then calibrated by comparing model hindcasts with reconstruction targets from the last interglacial period, the last glacial maximum and the mid-Holocene. Finally the calibrated DAIS model is validated against observations of recent AIS ice loss and the future applicability of the calibrated and validated model is discussed.

2 Model formulation and characteristics

The DAIS model builds upon the simple Oerlemans AIS model (Oerlemans, 2003, 2004, 2005, referred henceforth as O3, O4 and O5). The point of departure here is O5; a more detailed description is found in O3.

2.1 Mass balance

The Oerlemans model considers the mass budget of an axi-symmetrical ice sheet with ice sheet radius R resting on a bed with a constant slope, s, before ice loading. The undisturbed bed profile, b, is

$$b(r) = b_0 - sr \tag{1}$$

where r is the radial coordinate and b_0 is the (undisturbed) height at the center of the continent (all model parameters and their standard values are listed in Table 1). Ice loading depresses the bed to immediate isostatic equilibrium. Constant stress is assumed at the ice sheet base leading to a parabolic profile for the ice sheet surface height h in this perfect-plasticity limit:

$$h(r) = b_0 - sR + \{\mu(R - r)\}^{0.5} \tag{2}$$

GMDD
7, 1791–1827, 2014

where μ is a profile parameter related to ice stress (O3). Ice sheet evolution follows from conservation of mass:

$$\frac{dV}{dt} = B_{tot}(T_a, R) + F(SL, R) \quad (3)$$

where V is ice volume, B_{tot} is the total mass accumulation rate on the ice sheet and F is the total ice flux across the grounding line. The mean Antarctic temperature reduced to sea level, T_a, and sea level, SL, (relative to its 1961–1990 mean) are the only forcings in the original model. Following O5 I take present day $T_a = -18\,^{\circ}C$ (in the following present day refers to a 1961–1990 mean). The second term on the right hand side of Eq. (3) is only considered for a marine ice sheet, i.e. for $R > (b_0 - SL)s^{-1} = r_c$, the distance from the continent center to where the ice sheet enters the sea. I adopt the O5 approximation of equating the distance from the continent center to the grounding line with the ice sheet radius. Figure 1 shows a cross-section of a steady state solution of the model with standard parameter values and present day forcing.

The mass balance B at any height on the ice sheet surface is specified as

$$B = P \text{ for } h \geq h_R \text{ and } B = P - \beta(h_R - h) \text{ for } h < h_R \quad (4)$$

where $h_R(T_a)$ is the height of the runoff line above which precipitation, $P(T_a)$, is assumed to accumulate as snow and $\beta(P)$ is a rate of mass balance increase with height. Sublimation has been disregarded here. The problem can be easily reformulated in terms of an equilibrium height, h_e, where the yearly-mean mass balance is zero: from Eq. (4) $h_e = h_R - P/\beta$. Likewise total accumulation and total ablation can be calculated by integrating B over the ice sheet surface above and below h_e, respectively. Results from such a calculation will be presented below. However, integration of B over the whole surface to obtain B_{tot} is more straightforward for obtaining problem solutions (O3).

The mass balance part of the problem is closed by choosing appropriate expressions for h_R, P and β. For the runoff line height,

$$h_R = h_0 + cT_a \quad (5)$$

GMDD
7, 1791–1827, 2014

where values for h_0 and c are based on mass balance studies (O4). For precipitation,

$$P = P_0 \exp(\kappa T_a) \tag{6}$$

where P_0 is the (ice equivalent) precipitation at 0 °C and the value of the coefficient κ is chosen assuming a relationship between columnar water content (that increases exponentially with temperature) and precipitation. No attempt is made here (nor in O5) to deal with decreasing precipitation toward the center of the continent. This feature was included in O4 but at the cost of one extra free parameter. For the mass balance gradient β,

$$\beta = \nu P^{\frac{1}{2}} \tag{7}$$

where this relationship and the value of the parameter ν in O5 were also based on mass balance observations that reflect in part larger vertical precipitation gradients for greater precipitation (e.g. Oerlemans, 2008). Integration of B as formulated above over the ice sheet surface yields

$$B_{\mathrm{tot}} = \pi P R^2 - \pi\beta(h_{\mathrm{R}} - b_0 + sR)\left(R^2 - r_{\mathrm{R}}^2\right) - \frac{4\pi\beta\mu^{\frac{1}{2}}}{5}(R - r_{\mathrm{R}})^{\frac{5}{2}} + \frac{4\pi\beta\mu^{\frac{1}{2}}}{3}R(R - r_{\mathrm{R}})^{\frac{3}{2}} \tag{8}$$

where $r_{\mathrm{R}} = R - \mu^{-1}(h_{\mathrm{R}} - b_0 + sR)^2$ is the distance from the continent center to where the runoff line intersects the ice sheet surface. The last three terms in Eq. (8) are considered only when T_a is warm enough for runoff to occur, i.e. for $h_{\mathrm{R}} > 0$. For parameter values of Table 1, this occurs for $T_a > -15.48$ °C, about 2.5 °C warmer than present day.

Note that the signs of the last two terms of Eq. (8) differ from those in comparable Eqs. (16) and (18) of O3. This is due to sign errors in the original work. This correction leads to much reduced runoff and, for the O5 parameter values, an AIS model much less sensitive to climate at warm temperatures. Now deglaciation occurs at an Antarctic temperature about 22 °C higher than present and about 4 °C higher than in a 3-D thermomechanical model (Fig. 2; Huybrechts, 1993). One possible explanation for this

GMDD
7, 1791–1827, 2014

G. Shaffer

behavior is the β value of $\sim 0.001\,\mathrm{m}$ ice $\mathrm{m}^{-1}\,\mathrm{yr}^{-1}$ for O5 parameter values (calculated at 0 °C). This is a low value for the balance gradient compared to observations, even for dry polar climates (Oerlemans, 2008). To address this I doubled the O5 value of ν from 0.006 to $0.012\,\mathrm{m}^{-0.5}\,\mathrm{yr}^{-0.5}$ yielding a climate sensitivity at warm temperatures similar to the 3-D model (Fig. 2). Detailed agreement of the idealized DAIS model with the 3-D model can not be expected since the latter includes a representation of real Antarctic topography. Further improvements/adjustments of the model runoff formulation/calibration might be undertaken but I defer this to future work. Rather I opt here to concentrate on revised formulations of the other main component of the model: ice flux across the grounding line. This has been the dominant process for ice loss from Antarctica over ice age cycles and will continue to be so in the near future.

2.2 Ice flux at the grounding line

In the following I retain the above O5 mass balance treatment (but with the sign correction) as well as all O5 parameter values except for the revised value of ν and a slight increase of b_0 from 760 m to 775 m. As in O5, the parameter values are chosen to reproduce present day AIS volume, area, mean surface elevation and mass throughput (Table 1). The ice flux at the grounding line, F, is,

$$F = -\left(2\pi R \frac{\rho_\mathrm{w}}{\rho_\mathrm{i}} H\right) S \tag{9}$$

where ρ_w and ρ_i are water and ice densities, H is the water depth, and S is the ice speed. H and S should be thought of as some average around the ice sheet periphery over all ice streams. To the grounding line/ice sheet radius approximation mentioned above,

$$H = b_0 - sR + \mathrm{SL} \tag{10}$$

The ice flux problem was closed in O5 by assuming that the ice speed is related linearly to the water depth: $S = f_0 H$ where the value of constant of proportionality f_0 was chosen to reproduce present day AIS throughput (Table 1).

The two recent advances in our understanding of ice flow at the grounding line discussed in the Introduction call for a revision of the model ice speed formulation. First, I take ice flux at the grounding line to depend on water depth there raised to a power (Schoof, 2007). Second, I take melting at the base of a marine ice shelf to depend on the temperature difference between subsurface temperature of the adjacent ocean and temperature at the ice shelf base, the latter anchored to the freezing temperature of sea water. Modelling studies have yielded a range of such dependencies from linear to quadratic (e.g. Williams et al., 2002; Holland et al., 2008). Below I am guided mainly by the comprehensive, 3-D ocean general circulation model study of Holland et al. (2008) who find a quadratic dependency on this temperature difference for a wide range of shelf-slope topographies: the melt rate is found to be proportional to the product of ocean flow speed and ocean temperature beneath the ice shelf, both of which increase linearly with ocean warming. However I also touch upon results for a model version with a linear dependency on this temperature difference.

With the above motivations I choose to formulate the ice speed as follows:

$$S = f_0 \left[(1-\alpha) + \alpha \{ (T_o - T_f)/(T_{o,0} - T_f) \}^2 \right] H^\gamma / (b_0 - sR_0)^{\gamma - 1} \tag{11}$$

where T_o is the ocean subsurface temperature adjacent to the AIS, α is a partition parameter varying from 0 to 1 and γ is the power for the relation of ice flux to water depth varying from the value of 1 (O5) to 19/4 (Schoof, 2007). Furthermore, T_f is the freezing temperature of sea water, $T_{o,0}$ is a present day reference T_o and R_0 is a reference R. The value for $T_{o,0}$ was obtained as described in Appendix A and the value for R_0 was taken from the steady state solution of the O5 model ($\alpha = 0$; $\gamma = 1$) with present day forcing ($T_a = -18\,^\circ\mathrm{C}$; SL = 0; see below and Table 1). Note the scaling in Eq. (11) by present day ocean-ice shelf temperature difference and water depth at the

GMDD
7, 1791–1827, 2014

grounding line. This anchors the present day ice speed values for all α and γ values to the reference solution ice speed.

The conservation of mass is now

$$\frac{\mathrm{d}V}{\mathrm{d}t} = B_{\mathrm{tot}}(T_\mathrm{a}, R) + F(\mathrm{SL}, T_\mathrm{o}, R) \tag{12}$$

In addition to sea level, remote forcing of the ice sheet now also enters by way of ocean subsurface temperature T_o. Model formulation in terms of the independent variable R is completed by relating ice volume to R, taking into account immediate isostatic adjustment and the effect on this adjustment of the displacement of sea water by ice (O3):

$$V = \pi(1-\varepsilon_1)\left(\frac{8}{15}\mu^{\frac{1}{2}}R^{\frac{5}{2}} - \frac{1}{3}sR^3\right) - \pi\varepsilon_2\left\{\frac{2}{3}s\left(R^3 - r_\mathrm{c}^3\right) - b_0\left(R^2 - r_\mathrm{c}^2\right)\right\} \tag{13}$$

where ε_1 is $\rho_\mathrm{i}(\rho_m - \rho_\mathrm{i})^{-1}$, ρ_m is rock density and ε_2 is $\rho_\mathrm{w}(\rho_m - \rho_\mathrm{i})^{-1}$. The last term in curly brackets on the right hand side of Eq. (13) is only considered for a marine ice sheet ($R > r_\mathrm{c}$). Finally from Eq. (13),

$$\begin{aligned}\frac{\mathrm{d}V}{\mathrm{d}t} = &\left\{\pi(1-\varepsilon_1)\left(\frac{4}{3}\mu^{\frac{1}{2}}R^{\frac{3}{2}} - sR^2\right) - 2\pi\varepsilon_2(sR^2 - b_0R)\right\}\frac{\mathrm{d}R}{\mathrm{d}t}\\ &- 2\pi\varepsilon_2\left(r_\mathrm{c}^2 - \frac{b_0}{s}r_\mathrm{c}\right)\frac{\mathrm{d(SL)}}{\mathrm{d}t}\end{aligned} \tag{14}$$

where the last term within the curly brackets and the last term in the equation are only considered for a marine ice sheet. Note the sign correction in the last term in curly brackets as well as the extra term at the end of the equation when compared with the original derivation in Eq. (13) of O3.

2.3 Steady state solution properties

Figure 3 shows the distribution of AIS ice volume for two different steady state model solutions as functions of Antarctic temperature and sea level for ranges of T_a and SL

GMDD
7, 1791–1827, 2014

spanning glacial times into past (and future) global warming conditions. The steady state model ice volume for present day, yearly-mean Antarctic temperature and sea level ($T_a = -18\,^{\circ}$C, SL = 0) is 24.78×10^{15} m^3 (marked by "**x**" in the figure). As discussed in Sect. 3, present day ice volumes for transient model solutions slightly exceed this steady state value since these solutions are still responding to past temperature and sea level rises.

Figure 3a shows the steady state distribution of AIS ice volume for the original (but corrected) O5 model with the parameter values of Table 1. Each of the steady state solutions upon which the figure is based was obtained by a 100 kyr integration of the above time dependent model equations. Each such integration of this semi-analytical model with a one year time step takes a fraction of a second on a personal computer. Steady state ice volumes increase for warming by 5–7 °C above present day, reflecting increased snow fall and accumulation for increasing temperature. Volumes decrease rapidly for still warmer temperatures as summertime melting becomes important. For very warm temperatures, isolines of ice volume become horizontal as the ice sheet recedes out of the ocean, eliminating ice sheet dependency on sea level. Ice volume is greater during maximum glacial conditions with mean local temperatures about 10 °C colder and sea level about 130 m lower than present. Increased continental area is needed for reduced snowfall to balance ice flux at the grounding line then.

Figure 3b shows the steady state distribution of AIS ice volume for a preferred model configuration from the calibration in Sect. 4 (case 4 of Table 2; $\gamma = 2$, $\alpha = 0.35$ in Eq. 11). This configuration exhibits enhanced ice flux at the grounding line from 1. A higher-order ice flow dependency on water depth there and 2. Ice flow increase from ice shelf demise by way of basal melting. In this case the third forcing variable – high latitude, subsurface ocean temperature, T_o – also comes into play. For the calculations upon which this figure is based I used the following relationship that provided a good fit to the results in Appendix A:

$$T_o = 0.00690(T_a^2) + 0.439(T_a) + 6.39 \qquad (15)$$

GMDD
7, 1791–1827, 2014

For example, this yields $T_o = -0.50$, 0.72 and 3.32 °C for $T_a = -28$, −18 and −8 °C, respectively. Greater model dependency on sea level leads to less relative dependency of ice volume on temperature for cold temperatures (isolines more vertical). Furthermore, ice volume now decreases with warming above present day values. The increase in ice flux at the grounding line from warmer ocean subsurface temperatures, increased basal melting and increased ice shelf demise can keep up with increased snow fall and accumulation from warmer atmospheric temperatures without the need for ice sheet growth to reach that balance. Rather, ice sheet contraction is now needed for that balance as temperatures warm.

Figure 4 provides a closer look at ice conservation terms for steady state solutions of this preferred model configuration. The sum of total accumulation (a), total ablation (b) and total ice flux at the grounding line (c) add up to zero for each T_a, SL combination. As mentioned above, there is a balance between total accumulation and total ice flux for T_a less than −15.5 °C. Likewise, there is a balance between total accumulation and ablation for T_a greater than about −1 °C, at which point the ice sheet has receded out of the ocean. Total accumulation is greatest for T_a of about −5.5 °C, the temperature around which ablation and ice flux are of comparable importance. Ablation and ice flux are greatest for T_a of about −2 °C and −13 °C, respectively. All these terms increase as sea level decreases illustrating the effect of increased ice sheet area and circumference for a lower sea level.

3 Model calibration and validation

The strategy I use to obtain a first calibration of the DAIS model is to compare hindcasts of sea level equivalent (SLE) from waxing and waning of the model AIS over the last two glacial cycles to paleoreconstructions that provide constraints on this SLE. In particular I consider the period from 240 kyr BP up to the year AD 2010 (I take 0 BP to be AD 2000). The first step is to construct credible time series over this time period for the three model forcings: Antarctic temperature reduced to sea level, T_a, sea level

GMDD
7, 1791–1827, 2014

around Antarctica, SL, and subsurface ocean temperature around Antarctica, T_o. The forcing time series used here are shown in Fig. 5. A detailed description of how these series were constructed is given in Appendix A. The second step is to choose time slices for which suitable paloereconstructions are available. For this first calibration I choose to work with the last interglacial (LIG), the last glacial maximum (LGM) and the mid-Holocene (HOL) at about 6000 BP.

Maximum LIG sea level was considerably higher than present. Recent estimates have converged on a range of about 6–9 m above present for this maximum (Kopp et al., 2009; Dutton and Lambeck, 2012). Potential sources for the LIG sea level rise are ocean warming, melting mountain glaciers and ice caps and ice loss from Greenland and Antarctica. An LIG steric sea level rise of about 0.65 m follows from DCESS model calculations of ocean warming in Appendix A. Sea level would rise about 0.4 m for melting of all extant mountain glaciers and ice caps (Vaughan et al., 2013); their contribution to LIG sea level rise was probably considerably less than this for LIG global temperatures less than 2 °C above present day (Fig. A1). Taken together, these two sources can explain an LIG sea level rise of at most 1 m. The Greenland contribution to LIG sea level rise may have been in the range 2.0–2.5 m (Kopp et al., 2009; NEEM, 2013). The sum of these contributions leaves a remaining 2.5–5.5 m to be explained by ice loss from Antarctica. I adopt this range as my LIG constraint.

The Antarctic Ice Sheet was larger during the LGM. Ice sheet and glacial isostatic adjustment (GIA) modeling a decade ago indicated a range of 14–21 m SLE for this size increase (Clark and Mix, 2002; Peltier, 2004; Huybrechts, 2002). However, more recent modeling and GIA studies that consider local GPS observations show lower values of 8–10 m (Ivins and James, 2005; Whitehouse et al. 2012). This issue needs to be resolved but for present purposes I assume the range of 8–17 m SLE for my LGM constraint. By the mid-Holocene, the Northern Hemisphere ice sheets had melted and mean sea level had risen to about 2–3 m below present (Lambeck et al., 2010). Since temperatures had been slightly warmer than present for thousands of years by then (Marcott et al., 2013), the ocean may have been warmer and less ice than present may

GMDD
7, 1791–1827, 2014

have been present in mountain glaciers and ice caps and perhaps also on Greenland then (Vinter et al., 2009). These effects would have raised sea level to or slightly above present levels. Taken together with the mean sea level estimate, this implies an AIS size about 2–4 SLE above present. I adopt this range as my HOL constraint.

3.1 Hindcasts over the last two glacial cycles

Here I integrate the time dependent equations for ice sheet radius, R, from 240 kyr BP to AD 2010 for the forcing in Fig. 5 and for four different model setups (cases 1–4 in Table 2). The integrations start from the initial condition of $R = R_0$ (1.8636×10^6 m), the radius of the steady state model solution for present day, yearly-mean Antarctic temperature and sea level. This is an appropriate initial condition for the interglacial conditions at 240 kyr BP. Tests with other reasonable initial conditions varying by up to 10 % from the above value produced identical hindcasts from about 220 kyr BP onward. With the use of Eq. (13), ice sheet volume was then calculated and converted to SLE whereby an SLE of 57 m was taken to correspond to the ice volume of the above steady state model solution, 24.78×10^{15} m^3.

The model hindcast with the original (but corrected) Oerlemans model (case 1) exhibits a slow, low amplitude response to the forcing whereby maximum SLE occurs about 30 kyr after the last interglacial period (red lines in Fig. 6). In this setup the AIS continues to respond significantly at present to sea level rise over the last deglaciation and would continue to loose mass equivalent to more than 1 m SLE if present day temperature and sea level were maintained (Table 2). A model hindcast with increased sensitivity of ice flow to sea level rise (case 2) shows a more rapid, higher amplitude response, more in accord with the data constraints (maroon lines in Fig. 6). Now the timing but not the amplitude of SLE target at the LIG is achieved. As the model now responds more rapidly to sea level change, there is much less commitment to future sea level rise from continuing model response to the last deglaciation (Table 2). A model hindcast with increased sensitivity of ice flow to ocean subsurface temperature (case 3) shows a still higher amplitude, a good agreement with the SLE target at the LIG but a slow response to the last deglaciation (green lines in Fig. 6). Here almost all the AIS ice loss occurs after 10 kyr BP, the AIS ice volume is too large during the mid-Holocene and there is a future sea level rise commitment of nearly 2 m (Fig. 6; Table 2).

A model hindcast that incorporates both increased sensitivity of ice flow to sea level rise and to ocean subsurface temperature (case 4) meets all three reconstruction targets (blue lines in Fig. 6). The responses at both the LIG and the last deglaciation are now both sufficiently fast and large. Maximum SLE during the LIG was 3.07 m. When rerun using the original Waelbroeck et al. (2002) sea level curve across the LIG (Appendix A; Fig. 5), case 4 yields a somewhat lower maximum of 2.31 m. The results of cases 3 and 4 demonstrate that the key model feature for simulating an LIG-like ice loss is subsurface ocean temperature leading to ice flow acceleration. Ice loss from the AIS during the last deglaciation now occurs mainly after 15 kyr BP and includes a several meter SLE ice loss at melt water pulse 1A, forced by ocean subsurface warming and sea level rise across the pulse. This result is consistent with a mainly Northern Hemisphere source of this melt water event (e.g. Gregoire et al., 2012). The case 4 hindcast is also consistent with a reconstruction that places the 220 kyr BP sea level high stand several meters below present day sea level (Waelbrocke et al., 2002).

3.2 Comparison with past and present day estimates

Figure 7 shows the results of a more systematic search for the degree to which increased sensitivity of ice flow to sea level rise (as characterized by the parameter γ) and to ocean subsurface temperature (as characterized by the parameter α) lead to model hindcasts that satisfy all three reconstruction targets. From top to bottom panes, the figure shows isolines of Antarctic Ice Sheet SLE for the last interglacial, the last glacial maximum and the mid-Holocene, respectively, for model hindcasts spanning the ranges of γ and α. The four cases considered above are plotted as black dots. The isoline ranges of SLE defined by the reconstruction targets are shaded. Of the 336 hindcasts tested, 29 meet all three reconstruction targets (red dots in the figure). Acceptable values for α are 0.25–0.45 with the lower values constrained mainly by the

GMDD
7, 1791–1827, 2014

LIG target and the higher values mainly constrained by the LGM target. Acceptable values for γ are 1–3.75 and are mainly constrained by the HOL target. However most of the acceptable solutions are grouped in the γ range of 1.75–3. These values are somewhat lower than expected from boundary layer theory (Schoof, 2007) but it should be remembered that they represent some mean of all ice streams around Antarctica with varying degrees of buttressing from ice shelves. The low value outliers for γ are coupled to low value outliers for α.

The above results show some promise for the use of such well-calibrated versions of DAIS in other future applications. After all, the model captured well the timing and amount of ice loss during the warmer-than-present LIG and evidence has been growing for the importance of the process by which this loss occurred in the model – ice flow increase driven ultimately by subsurface ocean warming (Pritchard et al., 2012). However, the well-calibrated model versions should also pass verification tests whereby their hindcasts are compared with reconstructions outside of the calibration interval. Much recent effort has gone into quantifying the rate of ongoing sea level rise due to ice loss from Antarctica. The most recent IPCC estimate of this for the period AD 1993–2010 is $0.27 \pm 0.11\,\mathrm{mm\,yr^{-1}}$ (Vaughan et al., 2013). Figure 8 shows isolines of this rate for this period as calculated from the same model hindcasts as in Fig. 7. The isoline range defined by the recent IPCC estimate is shaded and the well-calibrated model setups from Fig. 7 are plotted in Fig. 8. There is a large overlap between the rate of ongoing sea level rise from AIS ice loss for these model combinations and the IPCC estimate. For example, the rise for case 4 is $0.24\,\mathrm{mm\,yr^{-1}}$ (Table 2). Only a few well-calibrated setups with low values of α and high values of γ fall outside the IPCC range.

I also tested a model version identical to the present one except for a linear, rather than quadratic, dependence of basal melting on the temperature difference between the subsurface temperature of the adjacent ocean and the temperature at the ice shelf base. With this version it was also possible to satisfy all three reconstruction targets but in a much narrower parameter space with acceptable values for α of 0.65–0.7 and for γ of 1.5–2. These few acceptable hindcasts produced rates of ongoing sea level rise

GMDD
7, 1791–1827, 2014

from AIS ice loss in the range of 0.24–0.31 mm yr^{-1}, also in good agreement with the recent IPCC estimate.

4 Discussion

Here I formulated a simple Antarctic Ice Sheet model by first adopting and making corrections to a published mass balance approach (Oerlemans, 2003, 2004, 2005) and then by advancing a new treatment of ice flow at the grounding line based on recent advances in our understanding of the controls on this flow. It was then possible to calibrate the resulting DAIS model, as forced by reconstructed Antarctic temperature, sea level and subsurface ocean temperature, such as to simultaneously satisfy reconstructions of the contributions of the AIS to sea level during the last interglacial, the last glacial maximum and the mid-Holocene. Finally it was shown that the well-calibrated model hindcasts also reproduced best estimates of the present rate of ongoing sea level rise from AIS ice loss. These results lend some support for the use of the present DAIS model for hindcasts farther back into the past as well as for projections into the future. However the question arises of how much confidence can be placed in the results of such a simple model. On one hand, well-calibrated simple models have proven useful in many contexts in the past (Shaffer et al. 2009; Meinhausen et al. 2009). On the other hand there are key questions regarding the AIS that can not be addressed in detail with the simple DAIS model. Perhaps the most emblematic of such questions regards the collapse of the West Antarctic Ice Sheet.

Analyses of sea level rise during the last interglacial period indicate that during this period AIS ice loss compared to present day was 2.5–5.5 m in sea level equivalent (Kopp et al., 2009; Dutton and Lambeck, 2012). The lower end of this estimate coincides with a recent calculation of how much sea level would rise from the collapse of the present day WAIS (3.3 m; Bamber et al., 2009.). The upper end of this estimate would require some additional contribution from East Antarctica. Basal melting in combination with a high order dependency of ice flow on grounding thickness facilitate marine

GMDD
7, 1791–1827, 2014

ice-sheet instability, such as would likely be active in a WAIS collapse, but would also increase flow in East Antarctic ice streams (Schoof, 2007; Joughin et al., 2012). Both basal melting and the high-order ice flow dependency were included, albeit schematically, in the DAIS model and made it possible for this simple model to simulate observed AIS ice loss during the LIG when forced by reconstructed ocean subsurface temperatures. Marine ice-sheet instability also requires complex bed geometry with the bed sloping downwards in the inland direction. As shown in Fig. 1, the depressed bed of the DAIS model slopes in this manner. However, assumed immediate isostatic adjustment in this highly-idealized model immediately restores the initial upward slope. While the model has been calibrated to produce observed LIG ice loss of the size of a WAIS collapse when forced with some realism, it can therefore not be expected to capture detailed timing of a marine ice sheet instability nor high, short-term ice loss rates that would be associated with one. Still, when calibrated with paleoconstraints the model was successful in reproducing present, short term rate of ice loss from the AIS.

Recently a much more complex and complete model of the AIS was used to address past collapses of the WAIS (Pollard and DeConto, 2009). A long hindcast of this model showed considerable skill in hindcasting the timing of such collapses when compared to the ocean sediment record. However, this hindcast also showed a large collapse in the next-to-last interglacial and a smaller one in the last interglacial, in conflict with sea level reconstructions (Waelbroeck et al., 2002: Kopp et al., 2009). The well-calibrated hindcasts of the DAIS model presented above (Fig. 6) captured correctly the relative amplitudes of AIS ice loss for these last two interglacials. Perhaps this difference in model hindcast behavior can be explained in that the complex model used deep-sea-core δ^{18}O and orbital insolation variations to parameterize ocean forcing whereas the DAIS model used actual ocean hindcasts, albeit simplified, for this forcing.

I conclude that the DAIS model can be used profitably with care in a number of possible applications. These include long hindcasts still farther back in time as well as integrated assessment modeling for the near future. The very fast, semi-analytical DAIS model is well suited as a component for the latter application by allowing extensive

GMDD
7, 1791–1827, 2014

sensitivity studies and parameter variations for deriving robust confidence intervals on projections. It should be remembered, however, that the model is well-calibrated and validated for conditions as warm as the last interglacial for which ice flux at the grounding line is essentially the only ice loss term. If future warming becomes sufficiently strong, ablation will also becomes an important factor in the mass balance of the Antarctic Ice Sheet. Further model calibrations/improvements may then be needed. Furthermore, as formulated, the DAIS model has limited skill, if any, in predicting the timing of any future collapse of the WAIS. But this is a limitation shared by many other more complex models of the Antarctic Ice Sheet.

5 Code availability

Matlab codes for the DAIS model, the 240 kyr forcing data and instructions for using the model can be downloaded from www.dcess.dk under "DCESS models".

Appendix A

Forcing reconstructions for the last two glacial cycles

For Antarctic temperature reduced to sea level, T_a, I use temperature anomaly reconstructions adjusted to a present day mean temperature of −18 °C (present day refers to the mean of the period AD 1961–1990). For the period 1500–240 000 BP, I adopt temperature anomaly estimates from the Dome C ice core (Jouzel et al., 2007) as referenced to 1.2 times the mean global temperature anomaly in the period 500–1500 BP from Mann et al. (2008). The factor 1.2 is an estimated interglacial polar amplification factor for Antarctica. This referencing led to a small adjustment of −0.1 °C relative to the published temperature anomalies. For the periods AD 500–1850 and AD 1851–2010 I used the global mean temperature anomaly from Mann et al. (2008) and Morice et al. (2012), respectively, multiplied by 1.2. These two time series have already been

Discussion Paper | Discussion Paper | Discussion Paper | Discussion Paper |

GMDD

7, 1791–1827, 2014

Formulation, calibration and validation of the DAIS model

G. Shaffer

Title Page
Abstract Introduction
Conclusions References
Tables Figures
◂◂ ▸▸
◂ ▸
Back Close
Full Screen / Esc
Printer-friendly Version
Interactive Discussion

referenced to present day global means. The composite time series for T_a was then interpolated to one year time steps and is shown in Fig. 5.

There are no detailed and reliable time series for sea level around Antarctica so I fall back upon global mean sea level estimates for SL. Reconstruction of a specific Antarctic sea level time series would require knowledge of the sources of sea level change over the two glacial cycles and subsequent application of non-eustatic corrections for changes in ice mass (e.g. Mitrovica et al., 2001). This is beyond the scope of the present paper. For the period 21–240 kyr BP, I adopt SL values from Waelbroeck et al. (2002) but with an adjustment for the last interglacial period (LIG). In this work, the transition of LIG sea level to levels above present day took place at about 124 kyr BP. However, subsequent work put that transition earlier, at 126 ± 1.7 kyr BP (Waelbroeck et al., 2008) and around 130 kyr BP (Dutton and Lambeck, 2012). I adjust this LIG transition to occur at about 127.5 kyr, consistent with the more recent work, and likewise adjust the Waelbroeck et al. (2002) curve by a corresponding amount back to the preceding glacial maximum (Fig. 5). For the period 7000–21 000 BP, I adopt SL values from Clark et al. (2012) that include representations of melt water events during the last deglaciation. For SL in the period 6000 BP to AD 1869, I use the sea level curve of Lambeck et al. (2010). For 6000–7000 BP, I interpolated linearly between values from the above two sources. Finally, for AD 1870–2010, I adopt SL values of Church and White (2011) adjusted to a present day value of zero. The composite time series for SL was then interpolated to one year time steps and is shown in Fig. 5.

High latitude, ocean subsurface temperature, T_o, enters the model as a forcing that ultimately modulates ice flow at the grounding line (see Sect. 2). It is a major challenge to construct a realistic time series for this temperature since it will depend on some combination of local and remote processes like local wind-driven upwelling/downwelling and Atlantic Meridional Overturning Circulation strength. Furthermore this temperature will vary around Antarctica. For this task I take a very simple approach that however is in tune with the scope of the present paper and model. First I construct a global mean atmospheric temperature anomaly (GMATA) time series from

GMDD
7, 1791–1827, 2014

240 000 BP until AD 2010. This time series is relative to the mean temperature of the reference period AD 1961–1990 and 0 BP is taken to be AD 2000. The GMATA series is based mainly on Antarctic and Greenland ice core data before 1500 BP (see details below), adopts a global reconstruction afterward (Mann et al., 2008) and finally adopts a reconstruction based on direct temperature observations after AD 1850 (Morice et al., 2012; Fig. A1a). Then I force the DCESS model ocean with low-mid (0–52°) and high (52–90°) latitude atmospheric temperature series constructed from the global series using amplification factors (0.928 and 1.266, respectively) and mean reference period temperatures (20.55 and −4.39 °C, respectively), all taken from DCESS model simulations (Shaffer et al., 2008; Fig. A1b). The subsurface ocean temperature, T_o, used for the forcing of the DAIS model is then taken to be the average temperature in the depth range 200–800 m of the high latitude ocean zone of the DCESS model (52–70° ; Fig. A1b and Fig. 5). The value for $T_{o,0}$ in Table 1 is the mean T_o for the period 1961–1990. Note that the DCESS model has only one high latitude zone but the poleward extent of that ocean zone matches the equatorward extent of Antarctica.

For the period 1500–122 400 BP temperature estimates are available from Antarctic and Greenland ice cores (Jouzel et al., 2007; Masson-Delmotte et al., 2006). The GMATA time series for this period is calculated as a mean of the two estimates after each is 1. referenced to the 1961–1990 period by referencing to the mean temperature anomaly in the period 500–1500 BP from Mann et al. (2008) and 2. divided by appropriate polar amplification factors. These factors were found to be 3 and 6 for Antarctica and Greenland, respectively, by fitting to the temperature reconstruction of Shakun et al. (2012) for the period 11 000–22 000 BP after that reconstruction was referenced to the 1961–1990 period by referencing to a ~ 5000 yr common period with the results of Marcott et al. (2013) (Fig. A1a). Lower amplification factors of 1.2 and 2.4, respectively, were adopted for the interglacial part of the 1500–122 400 BP period.

The temperature estimates for the Greenland ice core used above are not available before 122 400 BP. GMATA time series were constructed as above for earlier times but using other estimates for Greenland temperature. For the period 128 700–240 000 BP,

GMDD
7, 1791–1827, 2014

this temperature was estimated from a proxy based on methane data from an Antarctic ice core (Spahni et al., 2005). For this I used the relation $T = -51.5 + 0.0802\,[CH_4(\text{ppb})]$ from a linear regression of referenced Greenland temperature on Antarctic methane for the period 150–122 400 BP. I also tried several more sophisticated approaches included non-linear regression and applying the simple DCESS model module for atmospheric methane (Shaffer et al., 2008) but found no significant improvement over the simple linear regression in terms of modeled vs. observed Greenland temperature for this calibration period.

A different approach was required for the remaining period of 122 400–128 700 BP encompassing Termination II and much of the last interglacial as little guidance can be found in complex methane – Greenland temperature relationships at Termination I into the present interglacial (Spahni et al., 2005; Masson-Delmotte et al., 2006). A detailed study of Termination II from a variety of climate archives indicates that Greenland warming lags that of Antarctica with rapid warming commencing around 128 500 BP in the northern North Atlantic and reaching full interglacial levels by about 127 000 BP (Masson-Demotte et al., 2010). Guided by these results I extended the interglacial, Greenland ice core temperature at 122 400 BP back to 127 000 BP and applied a linear interpolation between that value at that time and the (methane-based) temperature at 128 700 BP.

Acknowledgements. I thank the following people for discussions and/or for supplying data: Peter Clark, Robert Kopp, Valerie Masson-Delmotte, Johannes Oerlemans, Mark Siddall, and Claire Waelbroeck. I included the non-linear dependency of ice flow on grounding thickness in response to a comment by Catherine Ritz on an earlier version of the model. This work was supported by Project CONICYT/FONDAP/15110009 (Chile).

GMDD

7, 1791–1827, 2014

References

Bamber, J. L., Riva, R. E. M., Vermeersen, B. L. A., and LeBrocq, A. M.: Reassessment of the potential sea-level rise from a collapse of the West Antarctic Ice Sheet, Science, 324, 901–903, 2009.

Church, J. A. and White, N. J.: Sea-level rise from the late 19th to the early 21st century, Surv. Geophys., 32, 585–602, 2011.

Church, J. A., Clark, P. U., Cazenave, A., Gregory, J., Jevrejeva, S., Levermann, A., Merrifield, M. A., Milne, G. A., Nerem, R. S., Nunn, P. D., Payne, A. J., Pfeffer, W. T., Stammer, D., and Unnikrishnan, A. S.: Sea Level Change. in: Climate Change 2013: The Physical Science Basis. Contribution of Working Group I to the Fifth Assessment Report of the Intergovernmental Panel on Climate Change, edited by: Stocker, T. F., Qin, D., Plattner, G.-K., Tignor, M., Allen, S. K., Boschung, J., Nauels, A., Xia, Y., Bex, V., and Midgley, P. M., Cambridge University Press, Cambridge, UK and New York, NY, USA, 2013.

Clark, P. U. and Mix, A. C.: Ice sheets and sea level of the Last Glacial Maximum, Quaternary Sci. Rev., 21, 1–7, 2002.

Clark, P. U., Shakun, J. D., Baker, P. A., Bartlein, P. J., Brewer, S., Brook, E., Carlson, A. E., Cheng, H., Kaufman, D. S., Liu, Z., Marchitto, T. M., Mix, A. C., Morrill, C., Otto-Bliesner, B. L., Pahnke, K., Russell, J. M., Whitlock, C., Adkins, J. F., Blois, J. L., Clark, J., Colman, S. M., Curry, W. B., Flower, B. P., He, F., Johnson, T. C., Lynch-Stieglitz, J., Markgraf, V., McManus, J., Mitrovica, J. X., Moreno, P. I., and Williams, J. W.: Global climate evolution during the last deglaciation, Proc. Natl. Acad. Sci. USA., 109, 1134–1142, 2012.

Dutton, A. and Lambeck, K.: Ice volume and sea level during the last interglacial, Science, 337, 216–219, 2012.

Gregoire, L. J., Payne, A. J., and Valdes, P. J.: Deglacial rapid sea level rises caused by ice-sheet saddle collapses, Nature, 487, 219–222, 2012.

Holland, P. R., Jenkins, A., and Holland, D. M.: The response of ice shelf basal melting to variations of ocean temperature, J. Climate, 21, 2558–2572, 2008.

Huybrechts, P.: The Antarctic ice sheet during the last glacial–interglacial cycle: a three dimensional experiment, Ann. Glaciol., 11, 52–59, 1990.

Huybrechts, P.: Glaciological modelling of the Late Cenozoic East Antarctic ice sheet: stability or dynamism?, Geogr. Ann., 75, 221–238, 1993.

GMDD

7, 1791–1827, 2014

Title Page
Abstract | Introduction
Conclusions | References
Tables | Figures
◀| |▶
◀ ▶
Back | Close
Full Screen / Esc
Printer-friendly Version
Interactive Discussion

Huybrechts, P.: Sea-level changes at the LGM from ice-dynamic reconstruction of Greenland and Antarctic ice sheets during glacial cycles, Quaternary Sci. Rev., 21, 203–231, 2002.
Huybrechts, P. and de Wolde, J.: The dynamic response of the Greenland and Antarctic ice sheets to multiple-century climatic warming, J. Climate, 12, 2169–2188, 1999.
Ivins, E. R. and James, T. S.: Antarctic glacial adjustment: a new assessment, Antarct. Sci., 17, 541–553, 2005.
Joughin, I., Alley, R. B., and Holland, D. M.: Ice-sheet response to oceanic forcing, Science, 338, 1172–1176, 2012.
Jouzel, J., Masson-Delmotte, V., Cattani, O., Dreyfus, G., Falourd, S., Hoffmann, G., Minster, B., Nouet, J., Barnola, J. M., Chappellaz, J., Fischer, H., Gallet, J. C., Johnsen, S., Leuenberger, M., Loulergue, L., Luethi, D., Oerter, H., Parrenin, F., Raisbeck, G., Raynaud, D., Schilt, A., Schwander, J., Selmo, E., Souchez, R., Spahni, R., Stauffer, B., Steffensen, J. P., Stenni, B., Stocker, T. F., Tison, J. L., Werner, M. and Wolff, E. W.: Orbital and millennial Antarctic climate variability over the past 800,000 years, Science, 317, 793–796, 2007.
Kopp, R. E., Simons, F. J., Mitrovica, J. X., Maloof, A. C., and Oppenheimer, M.: Probabilistic assessment of sea level during the last interglacial stage, Nature, 462, 863–867, 2009.
Lambeck, K., Woodroffe, C. D., Antonioli, F., Anzidei, M., Gehrels, W. R. Laborel, J., and Wright, A. J.: Paleoenvironmental records, geophysical modelling, and reconstruction of sea level trends and variability on centennial and longer timescales, in: Understanding Sea Level Rise and Variability, edited by: Church, J. A., Woodworth, P. L., Aarup, T., and Wilson, W. S., Wiley-Blackwell, Hoboken, NJ, USA, 61–121, 2010.
Mann, M. E., Zhang, Z. H., Hughes, M. K., Bradley, R. S., Miller, S. K., Rutherford, S., and Ni, F. B.: Proxy-based reconstructions of hemispheric and global surface temperature variations over the past two millennia, P. Natl. Acad. Sci. USA, 105, 13252–13257, 2008.
Marcott, S. A., Clark, P. U., Padman, L., Klinkhammer, G. P., Springer, S. R., Liu, Z., Otto-Bliesner, B. L., Carlson, A. E., Ungerer, A., Padman, J., Hee, F, Cheng, J., and Schmittner, A.: Ice-shelf collapse from subsurface warming as a trigger for Heinrich eventsc, P. Natl. Acad. Sci. USA, 108, 13415–13419, 2011.
Marcott, S. A., Shakun, J. D., Clark, P. U., and Mix, A. C.: A reconstruction of regional and global temperature for the past 11,300 years, Science, 339, 1198– 1201, 2013.
Masson-Delmotte, V., Dreyfus, G., Braconnot, P., Johnsen, S., Jouzel, J., Kageyama, M., Landais, A., Loutre, M.-F., Nouet, J., Parrenin, F., Raynaud, D., Stenni, B., and Tuenter, E.:

Past temperature reconstructions from deep ice cores: relevance for future climate change, Clim. Past, 2, 145–165, doi:10.5194/cp-2-145-2006, 2006.
Masson-Delmotte, V., Stenni, B., Blunier, T., Cattani, O., Chappellaz, J., Cheng, H., Dreyfus, G., Edwards, R. L., Falourd, S., Govin, A., Kawamura, K., Johnsen, S. J., Jouzel, J., Landais, A., Lemieux-Dudon, B., Lourantou, A., Marshall, G., Minster, B., Mudelsee, M., Pol, K., Roethlisberger, R., Selmo, E., and Waelbroeck, C.: Abrupt change of Antarctic moisture origin at the end of termination II, P. Natl. Acad. Sci. USA, 107, 12091–12094, 2010.
Meinhausen, M., Meinhausen, N., Hare, W., Raper, S. C. B., Frieler, K., Knutti, R., Frame, D. J., and Allen, M.: Greenhouse-gas emission targets for limiting global warming to 2 °C, Nature, 458, 1158–1162, 2009.
Mitrovica, J. X., Tamisiea, M. E., Davis, J. L., and Milne, G. A.: Recent mass balance of polar ice sheets inferred from patterns of global sea-level change, 409, 1026–1029, 2001.
Morice, C. P., Kennedy, J. J., Rayner, N. A., and Jones, P. D.: Quantifying uncertainties in global and regional temperature change using an ensemble of observational estimates: the HadCRUT4 dataset, J. Geophys. Res., 117, D08101, doi:10.1029/2011JD017187, 2012.
Naish, T., Powell, R., Levy, R., Wilson, G., Scherer, R., Talarico, F., Krissek, L., Niessen, F., Pompilio, M., Wilson, T., Carter, L., DeConto, R., Huybers, P., McKay, R., Pollard, D., Ross, J., Winter, D., Barrett, P., Browne, G., Cody, R., Cowan, E., Crampton, J., Dunbar, G., Dunbar, N., Florindo, F., Gebhardt, C., Graham, I., Hannah, M., Hansaraj, D., Harwood, D., Helling, D., Henrys, S., Hinnov, L., Kuhn, G., Kyle, P., Läufer, A., Maffioli, P., Magens, D., Mandernack, K., McIntosh, W., Millan, C., Morin, R., Ohneiser, C., Paulsen, T., Persico, D., Raine, I., Reed, J., Riesselman, C., Sagnotti, L., Schmitt, D., Sjunneskog, C., Strong, P., Taviani, M., Vogel, S., Wilch, T., and Williams, T.: Obliquity-paced Pliocene West Antarctic ice sheet oscillations, Nature, 458, 322–328, 2009.
NEEM community members: Eemian interglacial reconstructed from a Greenland folded ice core, Nature, 493, 489–494, 2013.
Oerlemans, J.: A quasi-analytical ice-sheet model for climate studies, Nonlin. Processes Geophys., 10, 441–452, doi:10.5194/npg-10-441-2003, 2003.
Oerlemans, J.: Antarctic ice volume and deep-sea temperature during the last 50 Myr: a model study, Ann. Glaciol., 39, 13–19, 2004.
Oerlemans, J.: Antarctic ice volume for the last 740 ka calculated with a simple ice sheet model, Antarct. Sci., 17, 281–287, 2005.

GMDD
7, 1791–1827, 2014

Oerlemans, J.: Minimal Glacier Models, Utrecht Publishing & Archiving Services, Universiteitsbibliotheek Utrecht, 91 pp., 2008.
Peltier, W. R.: Global glacial isostasy and the surface of the ice-age earth: the ICE-5G (VM2) model and GRACE, Ann. Rev. Earth Planet. Sci., 32, 111–149, 2004.
Pollard, D. and DeConto, R. M.: Hysteresis in Cenozoic Antarctic ice-sheet variations, Global Planet. Change, 45, 9–21, 2005.
Pollard, D. and DeConto, R. M.: Modelling West Antarctic ice sheet growth and collapse through the past five million years, Nature, 458, 329–332, 2009.
Pritchard, H. D., Ligtenberg, S. R. M., Gricker, H. A., Vaughan, D. G., van den Broeke, M. R., and Padman, L.: Antarctic ice-sheet loss driven by basal melting of ice shelves, Nature, 484, 502–505, 2012.
Rignot, E, Casassa, G., Goginemi, P., Krabill, W., Rivera, A., and Thomas, R.: Accelerated ice discharge from the Antarctic Peninsula following the collapse of Larsen B ice shelf, Geophys. Res. Lett., 31, L18401, doi:10.1029/2004GL020697, 2004.
Schoof, C.: Ice sheet grounding line dynamics: steady states, stability, and hysteresis, J. Geophys. Res., 112, F03S28, doi:10.1029/2006JF000664, 2007.
Shaffer, G., Olsen, S. M., and Bjerrum, C. J.: Ocean subsurface warming as a mechanism for coupling Dansgaard-Oeschger climate cycles and ice-rafting events, Geophys. Res. Lett., 31, L24202, doi:10.1029/2004GL020968, 2004.
Shaffer, G., Malskær Olsen, S., and Pepke Pedersen, J. O.: Presentation, calibration and validation of the low-order, DCESS Earth System Model (Version 1), Geosci. Model Dev., 1, 17–51, doi:10.5194/gmd-1-17-2008, 2008.
Shaffer, G., Olsen, S. M., and Pedersen, J. O. P.: Long-term ocean oxygen depletion in response to carbon dioxide emissions from fossil fuels, Nat. Geosci., 2, 105–109, 2009.
Shepherd, A., Wingham, D., and Rignot, E.: Warm ocean is eroding West Antarctic Ice Sheet, Geophys. Res. Lett., 31, L23402, doi:10.1029/2004GL021106, 2004.
Spahni, R., Chappellaz, J., Stocker, T. F., Loulergue, L., Hausammann, G., Kawamura, K., Flückiger, J., Schwander, J., Raynaud, D., Masson-Delmotte, V., and Jouzel, J.: Atmospheric methane and nitrous oxide of the late Pleistocene from Antarctic ice cores, Science, 310, 1317–1321, 2005.
Vaughan, D. G., Comiso, J. C., Allison, I., Carrasco, J., Kaser, G., Kwok, R., Mote, P., Murray, T., Paul, F., Ren, J., Rignot, E., Solomina, O., Steffen, K., and Zhang, T.: Observations: cryosphere. in: Climate Change 2013: The Physical Science Basis. Contribution of Working

Group I to the Fifth Assessment Report of the Intergovernmental Panel on Climate Change [Stocker, T. F., Qin, D., Plattner, G.-K., Tignor, M., Allen, S. K., Boschung, J., Nauels, A., Xia, Y., Bex, V., and Midgley, P. M. (eds.)]. Cambridge University Press, Cambridge, UK and New York, NY, USA, 2013.

Vinther, B. M., Buchardt, S.L., Clausen, H. B., Dahl-Jensen, D., Johnsen, S. J., Fisher, D. A., Koerner, R. M., Raynaud, D., Lipenkov, V., Andersen, K. K., Blunier, T., Rasmussen, S. O., Steffensen, J. P., and Svensson, A. M..: Holocene thinning of the Greenland ice sheet, Nature, 461, 385–388, 2009.

Vizcaíno, M., Mikolajewicz, U., Jungclaus, J., and Schurgers, G.: Climate modification by future ice sheet changes and consequences for ice sheet mass balance, Clim. Dynam., 34, 301–324, 2010.

Waelbroeck, C., Labeyrie, L., Michel, E., Duplessy, J. C., McManus, J. F., Lambeck, K., Balbon, E., and Labracherie, M.: Sea-level and deep water temperature changes derived from benthic foraminifera isotopic records, Quaternary Sci. Rev., 21, 295–305, 2002.

Waelbroeck, C., Frank, N., Jouzel, J., Parrenin, F., Masson-Delmotte, V., and Genty, D.: Transferring radiometric dating of the last interglacial sea level high stand to marine and ice core records, Earth Planet. Sc. Lett., 265, 183–195, 2008.

Whitehouse, P. L., Bentley, M. J., and Le Brocq, A. M.: A deglacial model for Antarctica: geological constraints and glaciological modelling as a basis for a new model of Antarctic glacial isostatic adjustment, Quaternary Sci. Rev., 32, 1–24, 2012.

Williams, M. J. M., Warner, R. V., and Budd, W. F.: Sensitivity of the Amery Ice Shelf, Antarctica, to changes in the climate of the Southern Ocean. J. Clim., 15, 2740–2757, 2002.

Table 1. Model parameters and their standard values.

Symbol	Description	Standard value
T_f	Freezing temperature of sea water	$-1.8\,^{\circ}$C
ρ_i	Ice density	$0.917\,\mathrm{g\,cm^{-3}}$
ρ_w	Sea water density	$1.03\,\mathrm{g\,cm^{-3}}$
ρ_m	Rock density	$4\,\mathrm{g\,cm^{-3}}$
b_0	Undisturbed bed height at the continent center	775 m
s	Slope of the undisturbed bed	6×10^{-4}
μ	Profile parameter for parabolic ice sheet surface	$8.7\,\mathrm{m}^{0.5}$
h_0	Runoff line height for mean Antarctic temperature reduced to sea level (T_a) equal to $0\,^{\circ}$C	1471 m
c	Proportionality constant for the dependency of runoff line height on T_a	$95\,\mathrm{m}\,(^{\circ}\mathrm{C})^{-1}$
P_0	Annual precipitation for T_a equal to $0\,^{\circ}$C	0.35 m ice
κ	Coefficient for the exponential dependency of precipitation on T_a	$4 \times 10^{-2}\,(^{\circ}\mathrm{C})^{-1}$
ν	Proportionality constant relating of decrease of runoff with height to precipitation	$1.2 \times 10^{-2}\,\mathrm{m}^{-0.5}\,\mathrm{yr}^{-0.5}$
f_0	Proportionality constant for ice flow at the grounding line	$1.2\,\mathrm{m\,yr^{-1}}$
$T_{a,0}$	Present day T_a reduced to sea level[a]	$-18\,^{\circ}$C
SL_0	Present day sea level[a]	0 m
$T_{o,0}$	Present day, high latitude ocean subsurface temperature[a]	$0.72\,^{\circ}$C
R_0	Reference ice sheet radius	1.864×10^{6} m
γ	Power for the relation of ice flux to water depth	1–19/4[b]
α	Partition parameter for effect of subsurface ocean temperature on ice flux	0–1[b]

[a] Present day refers to the mean for the period AD 1961–1990.

[b] Ranges over which values are chosen to configure specific model hindcasts.

GMDD
7, 1791–1827, 2014

Table 2. Results for specific model configurations.

Case	Description	Parameter values	Present day volume (10^{15} m^3)	SL rise commitment from AIS (m)	1993–2010 SL rise rate from AIS (mm yr^{-1})
1	Original Oerlemans model (with corrections)	$\gamma = 1$, $\alpha = 0$	25.28	1.15	0.15
2	Increased sensitivity of ice flow to sea level	$\gamma = 2$, $\alpha = 0$	24.97	0.44	0.07
3	Increased sensitivity of ice flow to ocean subsurface temperature	$\gamma = 1$, $\alpha = 0.35$	25.54	1.75	0.42
4	Increased sensitivity of ice flow to sea level and ocean subsurface temperature	$\gamma = 2$, $\alpha = 0.35$	25.01	0.53	0.24

GMDD
7, 1791–1827, 2014

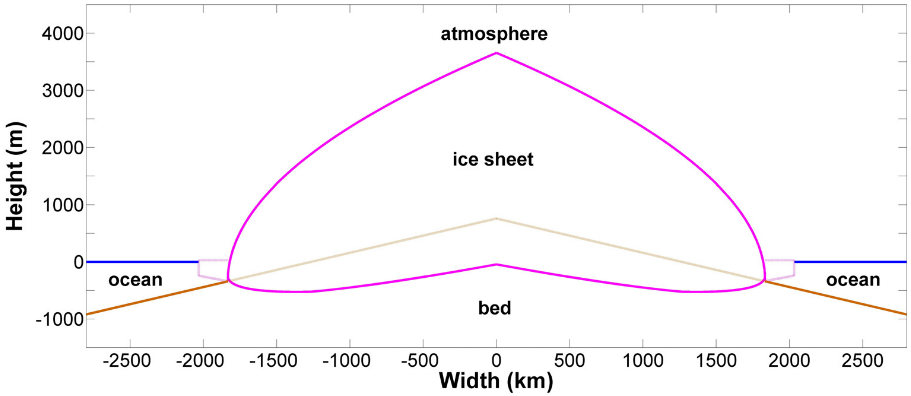

Fig. 1. Cross section of the steady state, DAIS model solution for present day Antarctic temperature, sea level and subsurface ocean temperature.

GMDD
7, 1791–1827, 2014

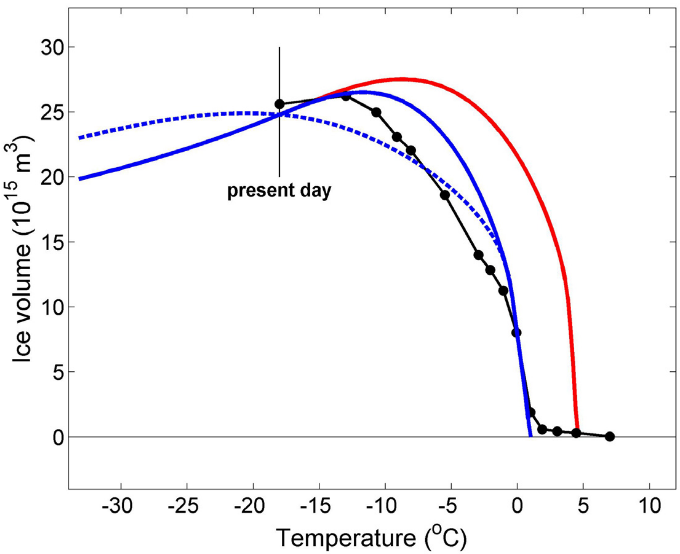

Fig. 2. Sensitivity of equilibrium solutions of DAIS model ice volume to Antarctic temperature reduced to sea level. Shown are solutions for the original (but corrected) Oerlemans (2005) model (Case 1, Table 2) for present day sea level (SL) and values for ν (Table 1) of 0.006 and 0.012 m$^{-0.5}$ yr$^{-0.5}$ (red and blue solid line, respectively) and for a preferred model setup (Case 4, Table 2) for present day SL and ocean subsurface temperature (blue dashed line). The black dots are comparable 3-D thermomechanical model solutions (Huybrechts, 1993).

GMDD
7, 1791–1827, 2014

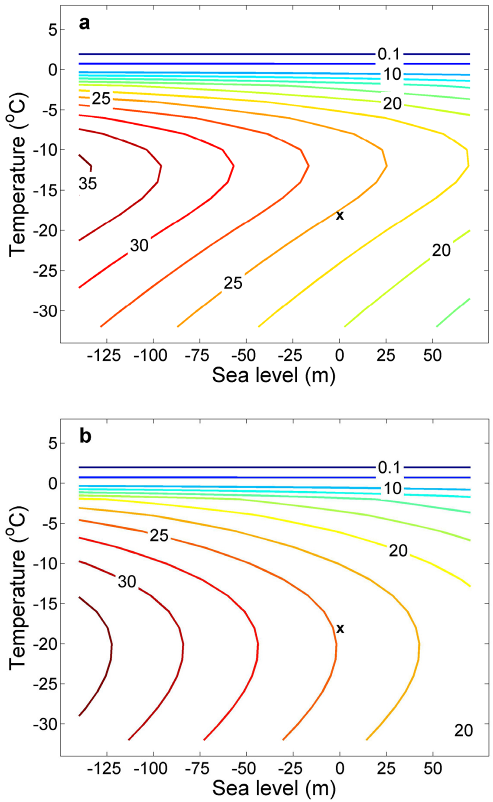

Fig. 3. Sensitivity of equilibrium solutions of DAIS model ice volume to Antarctic temperature (T_a) and sea level (SL). **(a)** Solutions for the original (but corrected) Oerlemans (2005) model and standard parameter values (Table 1; case 1 in Table 2). **(b)** Solutions for a preferred model setup (case 4 of Table 2) that also includes sensitivity to high latitude, subsurface ocean temperature (T_o) as calculated from Eq. (15). The black crosses mark solutions for present day T_a, SL and T_o (Table 1).

GMDD
7, 1791–1827, 2014

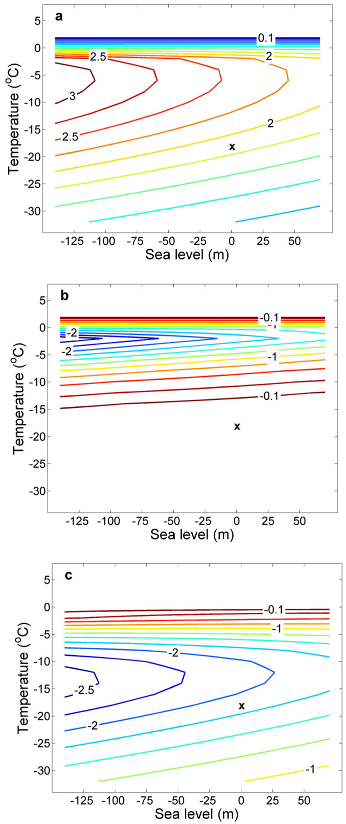

Fig. 4. Sensitivity of total equilibrium volume fluxes ($10^{12}\,m^3$ ice yr^{-1}) to Antarctic temperature, sea level and high latitude, subsurface ocean temperature for the preferred model setup (case 4 in Table 2). The volume fluxes are **(a)** Accumulation, **(b)** Ablation and **(c)** Ice flux at the grounding line. The black crosses mark solutions for present day T_a, SL and T_o (Table 1).

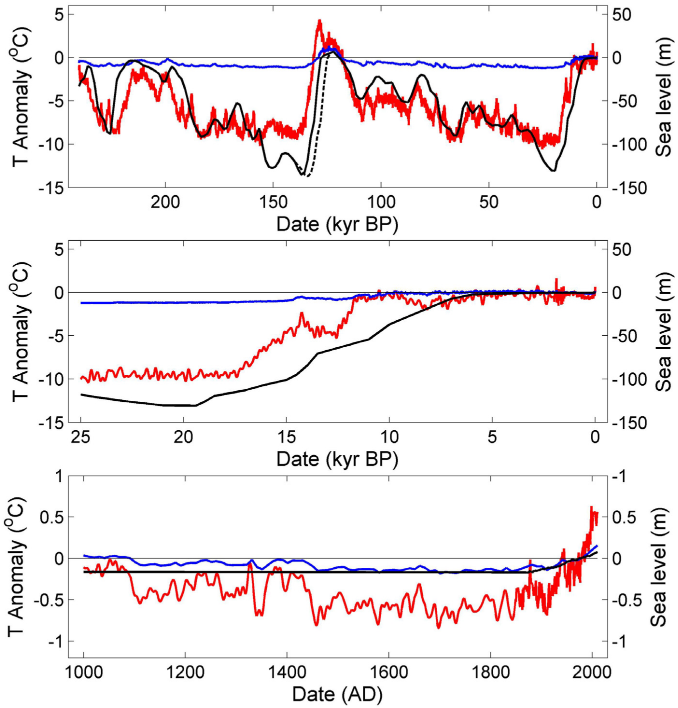

Fig. 5. Forcing for DAIS model hindcasts, reconstructed for the period 240 kyr BP to AD 2010 (see Appendix A for details). Shown are the anomalies of Antarctic temperature reduced to sea level (red lines), sea level (black lines) and high latitude, subsurface ocean temperature (blue lines), all relative to their present day values (−18 °C, 0 m and 0.72 °C, respectively). The actual forcings are the anomalies with the addition of these present day values. The lower two panes are blowups of portions of the full series (top pane). The dashed black line in the top pane shows the original Waelbroeck et al., (2002) sea level reconstruction for the period 140–122 BP (see discussion in Appendix A).

GMDD
7, 1791–1827, 2014

Formulation, calibration and validation of the DAIS model

G. Shaffer

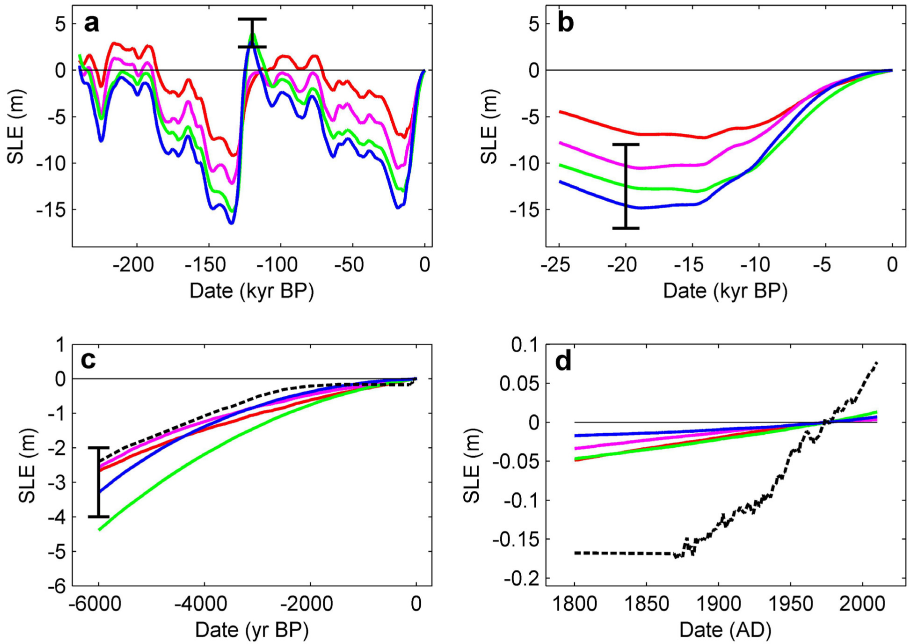

Fig. 6. Hindcasts of sea level equivalent (SLE) from changes in Antarctic Ice Sheet ice volume for the four model setups in Table 2 and for the period 240 kyr BP to AD 2010. The hindcasts are plotted relative to present day values (means for AD 1961–1990). Shown are results for the original (but corrected) Oerlemans (2005) model (case 1; red lines), a setup with increased sensitivity of ice flow to sea level (case 2, maroon lines), a setup with increased sensitivity of ice flow to ocean subsurface temperature (case 3, green lines) and a setup with increased sensitivity of ice flow to sea level and ocean subsurface temperature (case 4, blue lines). Frames **(b–d)** are blowups of the full hindcasts shown in **(a)**. Paleoreconstruction targets for the last interglacial, the last glacial maximum and the mid-Holocene are shown as vertical bars in **(a–c)**, respectively. Also shown is reconstructed global mean sea level from 6000 BP to the present (black dashed lines in **c** and **d**).

GMDD
7, 1791–1827, 2014

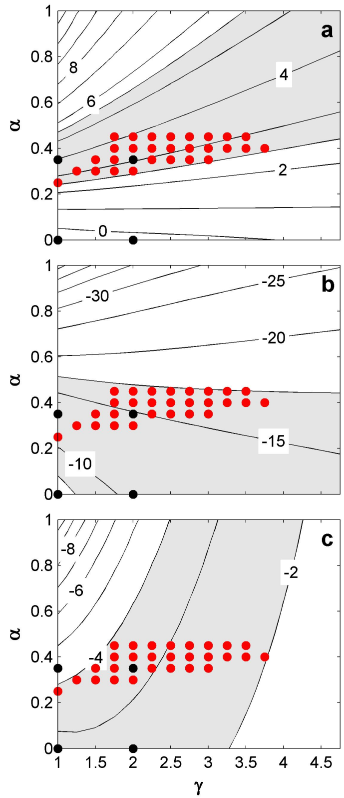

Fig. 7. Model hindcasts in specific time slices of sea level equivalent (m) from Antarctic Ice Sheet ice volume changes, as functions of model parameters γ and α. These parameters enter in the dependency of ice speed on water depth at the grounding line and on subsurface ocean temperature, respectively (see Eq. 11). The time slices are **(a)** the last interglacial period, **(b)** the last glacial maximum and **(c)** the mid-Holocene. Reconstruction targets for each time slice are shaded. The red dots mark hindcasts that meet all three reconstruction targets. The black dots mark the four hindcasts of Table 2 and Fig. 6.

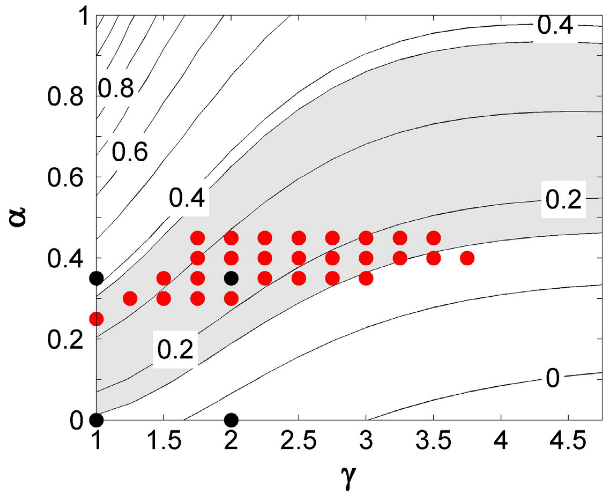

Fig. 8. Model hindcasts of the mean rate of sea level rise (mm yr^{-1}) from ice loss from the Antarctic Ice Sheet for the period AD 1993–2010 as functions of model parameters γ and α. The present IPCC best estimate for the range of this mean rate is shaded (Vaughan et al., 2013). The red dots mark hindcasts that meet all three paleoreconstruction targets (from Fig. 7). The black dots mark the four hindcasts of Table 2 and Fig. 6.

GMDD
7, 1791–1827, 2014

Title Page
Abstract Introduction
Conclusions References
Tables Figures
◂◂ ▸▸
◂ ▸
Back Close
Full Screen / Esc
Printer-friendly Version
Interactive Discussion

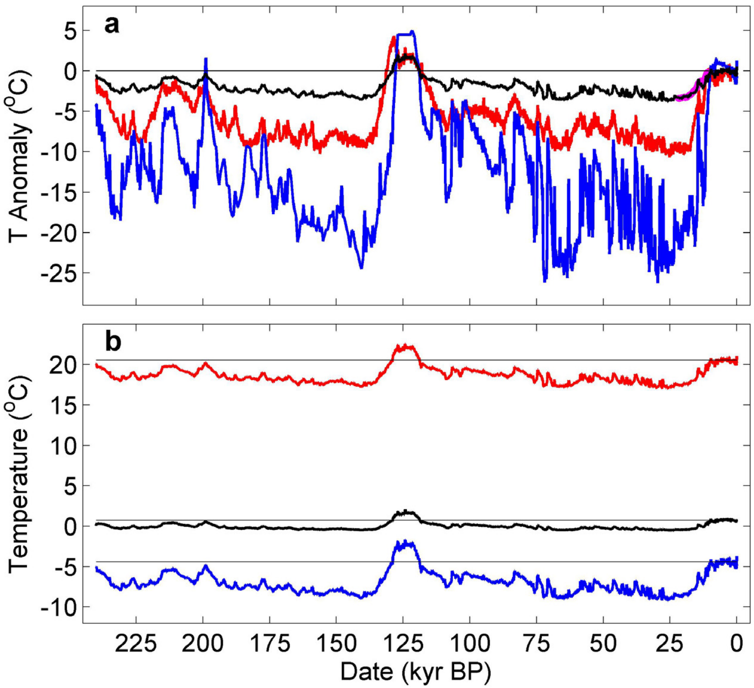

Fig. A1. Input time series and DCESS model results used in the construction of a high latitude, subsurface ocean temperature time series for forcing DAIS model hindcasts. Shown are **(a)** Antarctic and Greenland temperature anomalies (red and blue curves, respectively), a target time series for global mean temperature anomaly (short maroon line in upper right hand corner) and calculated global mean temperature (black line) and **(b)** Low-mid latitude and high latitude zone atmospheric temperatures used to force the DCESS model ocean (red and blue lines, respectively) and calculated high latitude, subsurface ocean temperature (black line). The thin horizontal black lines in **(b)** mark present day values (means for the period 1961–1990) for the respective time series. See Appendix A for details.